Carbohydrate Polymers 157 (2017) 57–64

Contents lists available at ScienceDirect

Carbohydrate Polymers

journal homepage: www.elsevier.com/locate/carbpol

Adsorption of divalent heavy metal ion by mesoporous-high surface area chitosan/poly (ethylene oxide) nanofibrous membrane

Md Islam Shariful, Sazzad Bin Sharif, Jacky Jia Li Lee, Umma Habiba, Bee Chin Ang, Muhammad Afifi Amalina*

Centre of Advanced Materials, Department of Mechanical Engineering, University of Malaya, 50603 Kuala Lumpur, Malaysia

ARTICLE INFO

Article history:
Received 17 June 2016
Received in revised form
19 September 2016
Accepted 20 September 2016
Available online 21 September 2016

Keywords:
Chitosan
Mesoporous fiber
Nanofiber
Adsorption

ABSTRACT

In this study, chitosan/poly (ethylene oxide) nanofibres were fabricated at different chitosan:PEO weight ratio by electrospinning process. The effects of chitosan/PEO composition onto adsorption capability for Cu(II), Zn(II) and Pb(II) ions were studied. Formation of beadless fibres were achieved at 60:40 chitosan:PEO ratio. Average fiber diameter, maximum tensile strength and the specific surface area of the beadless fibres were found to be 115 ± 31 nm, 1.58 MPa and 218 m^2/g, respectively. Chitosan/PEO composition that produced beadless fibres tend to possess higher hydrophilicity and maximum specific surface area. These characteristics lead the beadless fibres to the maximum adsorption capability. Adsorption equilibrium data were analysed by Langmuir and Freundlich isotherm. Freundlich isotherm showed the better fit with the experimental data and proved the existence of the monolayer adsorption conditions. The maximum adsorption capacity of the beadless fibres for Cu(II), Zn(II) and Pb(II) ions were found to be 120, 117 and 108 mg g^{-1}, respectively.

1. Introduction

To meet the demands of steep increase in population, world is leading towards modernization, specifically industrialization. Over the past century, for the sake of industrialization chemical, textiles, mining, agriculture, cosmetics, paper and leather introduced a large number of chemical substances into environment. Among those water pollutants in the form of dyes or metal ion pose serious threat to human health. Consuming heavy metals by water consumption can destroy the ultimate nervous system, may lead to skin allergies, kidney dysfunction and can increase the risk of cancer (Järup, 2003). Therefore it is abundantly important to remove the heavy metals from contaminated water sources. Adsorption is potentially the most suitable technique for heavy metal separation due to its effectiveness, regeneration easiness and inexpensive nature (Irani, Amjadi, & Mousavian, 2011; Lin & Chang, 2014; Liu & Wang, 2014). Among the available adsorbents nanofibrous membrane possess great interest from the researchers due to their high specific surface area and porous structure (Haider & Park, 2009; Thavasi, Singh, & Ramakrishna, 2008; Xiao et al., 2011). Electrospun fibres possess very high specific surface area and good porous structure (Deitzel, Kleinmeyer, Harris, & Tan, 2001) thus they are commonly used for adsorption. Among the natural polymers, chitosan, one kind of polysaccharides is interesting to explore for the application for the heavy metal ions removal due to its availability in nature and special properties like biocompatibility, biodegradability, non-toxicity and metal ion chelation. However, it is very difficult to fabricate pure chitosan nanofibres by electrospinning because of its inter and intra molecular interactions, complex chemical structure and polycationic nature in solution (Hardiansyah, Tanadi, Yang, & Liu, 2015; Hassiba et al., 2016; Kohsari, Shariatinia, & Pourmortazavi, 2016). In addition, the repulsive force of ionic groups of chitosan hinders continuous fibre formation (Min et al., 2004). Therefore, to improve the electrospinability, chitosan is usually blended with other synthetic or natural polymers, like poly (vinyl alcohol) (Duan et al., 2006; Koosha, Mirzadeh, Shokrgozar, & Farokhi, 2015), poly (ethylene oxide) (Bhattarai, Edmondson, Veiseh, Matsen, & Zhang, 2005; Li et al., 2015), poly acrylamide (Desai & Kit, 2008) and silk (Cai et al., 2010).

In general, the adsorption capability of electrospun membrane is mostly influenced by the specific surface area and porous structure of the membrane. Therefore, one of the aims of this study is to fabricate nanofibrous membrane having mesopores and high spe-

* Corresponding author at: Department of Mechanical Engineering, Faculty of Engineering, University of Malaya, Malaysia.
E-mail addresses: sharifulislam.mamun@gmail.com (M.I. Shariful), sbsjoh@yahoo.com (S.B. Sharif), jacky_ljl@hotmail.com (J.J.L. Lee), habiba_buet@yahoo.com (U. Habiba), amelynang@um.edu.my (B.C. Ang), amalina@um.edu.my (M.A. Amalina).

http://dx.doi.org/10.1016/j.carbpol.2016.09.063
0144-8617/

cific surface area by blending PEO with chitosan at different weight ratio. Though some researchers have already reported the fabrication of chitosan nanofiber by blending with PEO, to the best of our knowledge there is lack of information regarding the effect of chitosan/PEO composition onto adsorption capability of the membrane. Thus the focus of this study is to investigate the effect of chitosan/PEO composition towards the adsorption capability. Best composition of the chitosan/PEO nanofiber (CPNM) was determined in terms of the diameter size, number of beads per unit area and adsorption capability. The effects of contact time, different initial concentration, and adsorbent dosage on the adsorption of metal ions adsorption ability were analysed for the best composition. Furthermore, the adsorption kinetics and isotherms parameters were calculated to determine the character of the adsorption process. Lastly the reusability of the membrane was evaluated.

2. Experimental

2.1. Materials

In this study chitosan (M_w = 250000) and PEO (M_w = 900000) were employed to fabricate the nanofibrous membrane. Copper nitrate ($Cu(NO_3)_2$), zinc chloride ($ZnCl_2$) and lead nitrate ($Pb(NO_3)_2$) were used as the source of heavy metals. Heavy metals, acetic acid (CH_3COOH) and chitosan were purchased from Sigma-Aldrich (Malaysia). PEO was obtained from Kuraray Co. Ltd. (Tokyo, Japan).

2.2. Electrospinning process

Chitosan (4 wt%) and PEO (3 wt%) were dissolved in 80 wt% acetic acid solution and distilled water respectively. The mixtures were stirred for 24 h for complete dissolving of polymer. These two polymer solution were mixed at different chitosan/PEO weight ratios (40:60- S_1, 50:50-S_2, 60:40-S_3, 70:30-S_4, and 80:20-S_5). The electrospinning setup consisted of a high voltage power supply 25 kV (LD Didactic GmbH, Germany), a syringe pump NE-300 (New Era Pump Systems, NY, USA) and a stainless steel made stationary collector.

2.3. Characterization

The morphology of CPNM was examined by Desktop Phenom Pro-X scanning electron microscope (SEM). Average fiber diameter was determined by average of 100 diameter readings from 50 images at different spots. Intra fiber pores and porous nature of the membrane were demonstrated by Field emission scanning electron microscope (FESEM). Mechanical properties of the membrane was determined by Shimadzu AGS-X Series Universal Tensile Testing Machine with 50N load cell. Fourier transform infrared spectroscopy (FTIR) (Spectrum 400, Perkin-Elmer, USA) was employed to examine the chemical structures of the fibres and to confirm the formation of chitosan/PEO hydrogen bonding. X-ray diffraction (XRD) patterns were recorded using PANalytical Empyrean X-ray diffractometer with mono- chromated CuK_α radiation (λ = 1.54056A°), and a scanning rate of 0.1° s^{-1} over a 2θ range from 5° to 40°. The pore structure characteristics of CPNM were determined by N_2 adsorption-desorption isotherms by a Sorptomatic 1990. During the experiment, CPNM was degassed at 80 °C for 12 h, in a vacuum condition. The BET surface area was determined by the standard BET equation applied in the relative pressure range from 0.01 to 1.0. The total pore volume was calculated at a relative pressure of approximately 0.985 and at this relative pressure all pores were completely filled with nitrogen gas. The water contact angle was measured by using a goniometer Ramé-Hart Model 500 (Ramé-Hart Instrument Co., USA) at room temperature. The concentration of the residual colour of metal ion was measured in terms of absorbance by a Carian VARY 50 probe type UV–vis spectrophotometer.

2.4. Investigation of adsorption process

Metal ion adsorption experiments were carried out by soaking 50 mg of CPNM in 20 ml of the specified metal ion solution. In this study, copper nitrate ($Cu(NO_3)_2$), zinc nitrate ($Zn(NO_3)_2$) and lead nitrate ($Pb(NO_3)_2$) solutions are used in a batch mode. The parameters for the original adsorption experiments are as follows: 50 mg dosage, 50 mg/l initial concentration and 25 °C room temperature. pH value of the solution was controlled by adding 0.1 mol l^{-1} HCl or NaOH. pH values were measured using a pH meter.

The amount of metal ion adsorbed onto the nanofibrous membrane was calculated by the following equation (Dotto & Pinto, 2011):

$$q_t = \frac{C_0 - C_t}{m} V \quad (1)$$

Where C_0 and C_t represents the initial metal ion concentration and concentration at time t in (mg l^{-1}), V is the volume in litre (L) and m is the weight of nanofibrous membrane in gram (g).

Also, the metal ion removal (%) was calculated by the following equation (Chakraborty, Chowdhury, & Saha, 2011):

$$RE\,(\%) = \frac{C_0 - C_e}{C_0} \times 100 \quad (2)$$

2.4.1. Adsorption kinetics

In this study two adsorption kinetic models were being explored to demonstrate the controlling mechanism of the metal ion adsorption onto CPNM. First one is the Lagergren first order kinetic model. The linear form of this model is defined as (Sun, Liu, Jing, & Wang, 2015):

$$\log(q_e - q_t) = \log q_e - \frac{k_1 t}{2.303} \quad (3)$$

Where, q_e and q_t represents the amount of metal ion adsorbed (mg/g) at equilibrium and at time t respectively. k_1 (min^{-1}) is the Lagergren rate constant. Values of q_e and k_1 at different initial concentrations for all metal ions have been calculated respectively from the slope and intercept of the plots of log ($q_e - q_t$) versus t.

Pseudo second order kinetic model is the other model used in this study. The linear form of this model is (Cui et al., 2015):

$$\frac{t}{q_t} = \frac{1}{k_2 q_e^2} + \frac{t}{q_e} \quad (4)$$

Where, k_2 is the pseudo second order rate constant in (g/mg/min). Values of k_2 and q_e have been calculated respectively from the slope and the intercept of the plots of t/q_t versus t.

As the values of k_1, k_2 and q_e were calculated from linear regression, which has inherent bias effect, it is important to calculate the non-linear regression Chi-square (χ^2) to standardise the fitting quality. It can be calculated using the following equation (Ho, 2004).

$$\chi^2 = \sum \left| \frac{(q_e - q_{e.cal})^2}{q_{e.cal}} \right| \quad (5)$$

Where, q_e is the amount of metal ion adsorbed (mg/g) at equilibrium and $q_{e.cal}$ is the amount of metal ion adsorbed (mg/g) obtained from the two kinetic models. Therefore the best fitted kinetic model can be chosen by the lowest Chi- square (χ^2) value and highest regression co-efficient (R^2) value.

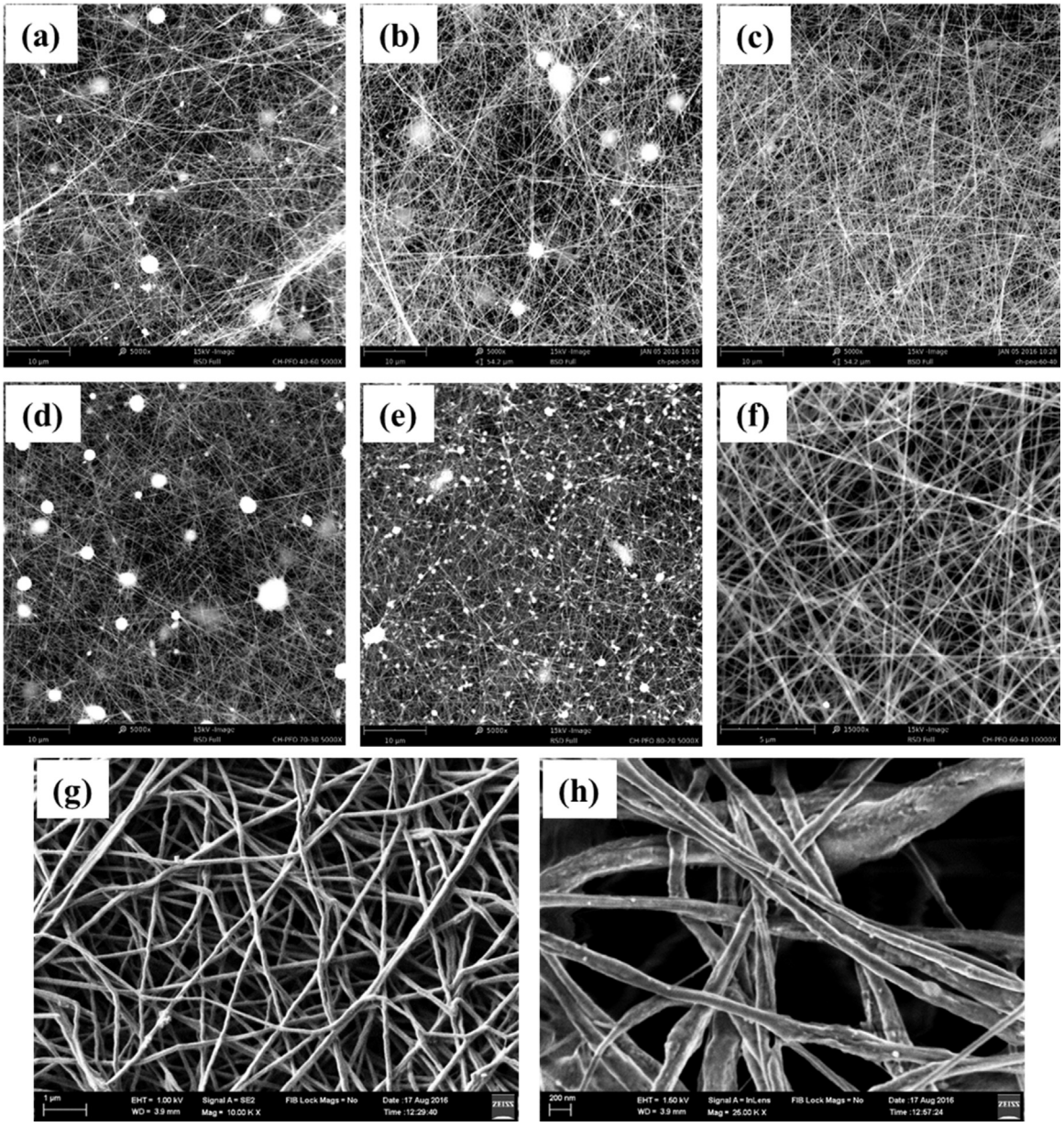

Fig. 1. SEM micrographs of CPNM (a) S_1 (b) S_2 (c) S_3 (d) S_4 and (e) S_5 at 5000×, (f) S_3 at 15000× and FESEM micrographs of (g) Intra fiber pores of S_3 and (h) rough surface of S_3.

2.4.2. Intra particle diffusion

To know the mechanism of the adsorption process, Weber and Morris (Han et al., 2010) proposed an adsorption model, which is renowned as Intraparticle diffusion model. The linearized form of this model is as follows:

$$q_t = k_{id} t^{\frac{1}{2}} + C \tag{6}$$

Where, C and k_{id} represent the boundary layer effect and the intra-particle diffusion rate constant, respectively. The values of k_{id} and C have been calculated from the slope and intercept of the second linear portion of the plots of q_t versus $t^{1/2}$ respectively. Boundary layer diffusion co-efficient (k_s) in min^{-1} can be calculated from the slope of the plots of C_t/C_0 versus t. Here C_t and C_0 denotes the concentration of metal ion in mg/l at time t and the initial concentration. The k_s values were calculated from the equilibrium data those were recorded before 20 min.

2.4.3. Adsorption isotherms

In this study, Freundlich and Langmuir isotherms were used to describe the reaction of metal ions with CPNM surface. The linear form of Freundlich isotherm is as follows (Mi, Wu, & Chen, 2015):

$$ln q_e = ln K_F + \frac{1}{n} ln C_e \tag{7}$$

Where, K_F and n are Freundlich constant indicating the capacity of the adsorbent ($mg\,g^{-1}$) and the intensity of the adsorption process. K_F and n values were calculated from the intercept and slope of the linear plot of $ln\ q_e$ versus $ln\ C_e$.

The linear form of Langmuir isotherm is (Mi, Wu, & Chen, 2015):

$$\frac{C_e}{q_e} = \frac{C_e}{q_m} + \frac{1}{K_L q_m} \tag{8}$$

Where, q_m is the monolayer capacity of the adsorbent ($mg\,g^{-1}$), K_L is the Langmuir constant ($l\,mg^{-1}$). q_m and K_L values were calculated

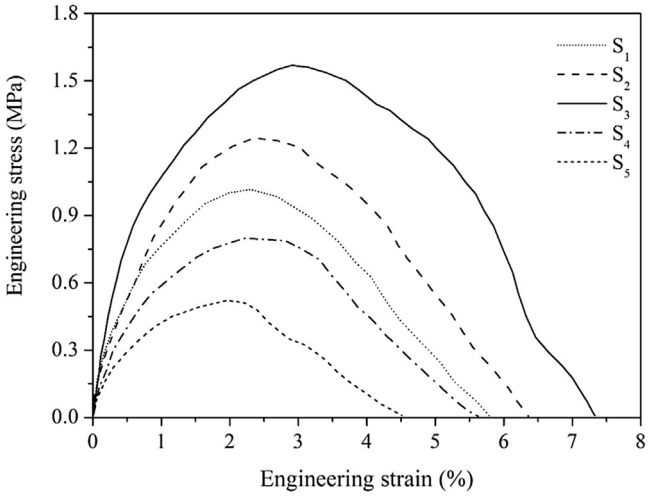

Fig. 2. Stress-strain curves of CPNM.

respectively from the slope and intercept of the plots of C_e/q_e versus C_e.

The favourability of Langmuir isotherm for equilibrium data can be predicted by dimensionless constant separation factor R_L. It can be calculated by the following equation (Ozdemir, Armagan, Turan, & Celik, 2004):

$$R_L = \frac{1}{1 + K_L C_m} \quad (9)$$

Where, C_m is the maximum initial concentration of the metal ion.

3. Results and discussion

3.1. Characterization of CPNM

3.1.1. Surface morphology analysis of CPNM

The morphology of CPNM is shown in Fig. 1. The parameters for the electrospinning process in different composition are tabulated in Table 1. The average fiber diameter was increased with increasing chitosan content. Availability of higher number of cations and electric charges with the increase of chitosan content is the principal reason for this (Talebian, Afifi, & Khanlou, 2014). Moreover, for electrospinning higher chitosan content solution, higher voltage is required. Higher voltage also responsible for higher fiber diameter (Huang, Zhang, Kotaki, & Ramakrishna, 2003). From Fig. 1(c) and (f), S_3 contains no bead with the average fiber diameter 115 ± 31 nm, whereas the surface of other samples contain large number of beads. Furthermore, intra fiber pores of S_3 are clearly visible in Fig. 1(g) and (h). Rough surface morphologies are observed in Fig. 1(h) which can be contributed towards higher surface area.

3.1.2. Mechanical properties of CPNM

The stress-strain curves of the CPNM samples are shown in Fig. 2. The experiment was conducted in a strain rate of 0.0001 s^{-1} for a sample size of 1 cm × 6 cm with a gauge length of 3 cm. The ultimate tensile strength of S_1, S_2, S_3, S_4 and S_5 were found to be 1.01, 1.25, 1.58, 0.79 and 0.52 MPa. S_5 having maximum beads exhibited the lowest mechanical strength, since beaded fiber tend to have lower mechanical strength (Gaharwar et al., 2014), where S_3 having no bead showing the highest mechanical strength.

3.1.3. Determination of the formation of hydrogen bonding

To determine the formation of hydrogen bonding between chitosan and PEO, FTIR and XRD analysis were carried out on pure chitosan, pure PEO and S_3. FTIR spectroscopy in a frequency range

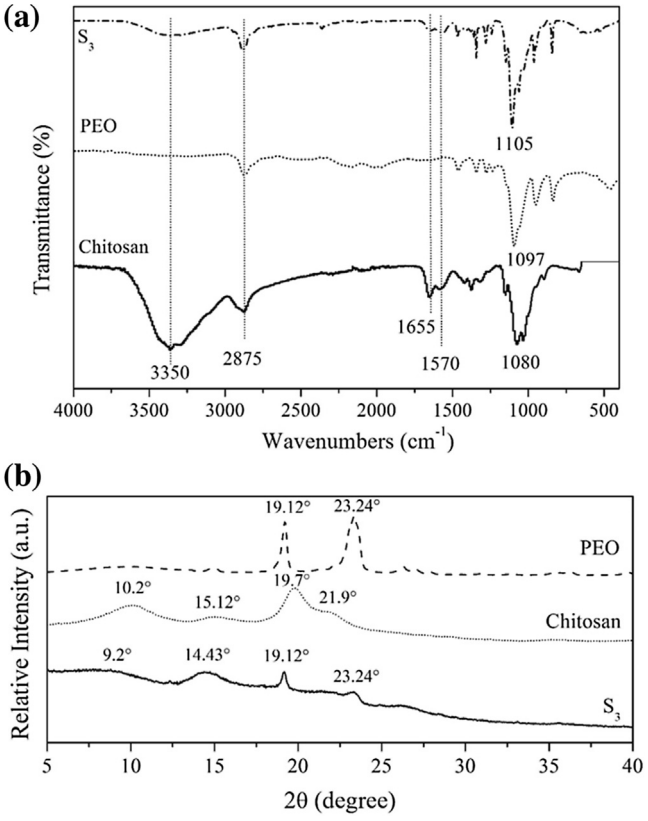

Fig. 3. (a) FTIR spectra and (b) XRD patterns of Chitosan, PEO and S_3.

of (4000–400) cm^{-1} of chitosan can be employed to determine the degree of deacetylation. According to Domszy and Roberts (Domszy & Roberts, 1985) the Eq. (10) can be used for determining the DD.

$$DD = 100 - [\frac{A_a}{A_b} \times \frac{100}{1.33}] \quad (10)$$

Here, A_a/A_b denotes absorption/transmittance band ratio. Several absorption band ratios such as A_{1580}/A_{2875}, A_{1655}/A_{2875}, A_{1655}/A_{3350}, A_{1320}/A_{3450}, A_{1655}/A_{1070}, A_{1655}/A_{1030}, A_{1580}/A_{1160}, and A_{1320}/A_{1420} have been proposed by researchers to determine the DD (Dong et al., 2002; Miya, Iwamoto, Yoshikawa, & Mima, 1980; Muzzarelli, Tanfani, Scarpini, & Laterza, 1980; Sannan, Kurita, Ogura, & Iwakura, 1978; Shigemasa, Matsuura, Sashiwa, & Saimoto, 1996). In this study A_{1650}/A_{3350} peak ratio was used. The calculated DD of chitosan was 70%.

In Fig. 3(a) pure chitosan shows a broad peak at 3350 cm^{-1}, that corresponds to N—H and hydrogen bonded O—H stretching vibration (Rakkapao, Vao-soongnern, Masubuchi, & Watanabe, 2011). The peaks at 897, 1060 and 1160 cm^{-1} prove the presence of saccharide group (Homayoni, Ravandi, & Valizadeh, 2009). Two peaks at 1570 and 1655 cm^{-1} represent $-NH_2$ (bending vibration, amide II) and C=O—NHR (amide I). The peak at 2875 and 1080 cm^{-1}, were attributed to the $-CH_2$ stretching and anti-symmetric stretching of C—O—C bridge. Pure PEO shows relatively sharp peak at 2885 cm^{-1}, which was attributed to $-CH_2$ stretching. And the peak at 1097 cm^{-1} represents C—O—C stretching. S_3 shows a sharp peak at 2875 cm^{-1}, which corresponds to $-CH_2$ stretch (Rakkapao, Vao-soongnern, Masubuchi, & Watanabe, 2011). The intensity of this peak increased as compared to pure PEO. The broad peak in the region of (3100–3300) cm^{-1} corresponds to N—H and O—H stretching vibration. The intensity of this peak decreased compared to pure chitosan. Other characteristic peaks shown by S_3 are 1105 and 962 cm^{-1}, represent vibration of ether group. By adding PEO, peak shifting was noticed at S_3 as compared to chitosan. The vibra-

Table 1
Parameters of electrospinning at different composition.

Sample name	Feed rate (ml/h)	Voltage (kV)	Average fiber diameter (nm)	No. of beads (beads/10 μm^2)
S_1	0.5	7	88 ± 19	7
S_2	0.4	8	101 ± 33	5
S_3	0.3	10	115 ± 31	0
S_4	0.15	12	131 ± 45	13
S_5	0.10	15	142 ± 52	41

Table 2
Metal ion removal (%) by CPNM after 60 min.

Sample name	Removal (%)		
	Cu(II)	Zn(II)	Pb(II)
S_1	89	83	76
S_2	92	85	78
S_3	96	91	83
S_4	81	74	71
S_5	72	63	61

tion bands at 1570, 1655 and 3350 cm^{-1} shifted to 1561, 1661 and 3358 cm^{-1}, respectively at S_3. This peak shifting and change in the intensity of the characteristic peaks may be because of the decrease of intermolecular hydrogen bonding of chitosan and forming new hydrogen boding between chitosan and PEO molecules (Chen, Mo, He, & Wang, 2008).

From Fig. 3(b), PEO showed its characteristic peaks at 2θ = 19.12° and 23.24° (Pittarate, Yoovidhya, Srichumpuang, Intasanta, & Wongsasulak, 2011). Chitosan showed major crystalline peak at 2θ = 10.2° and 19.7° that corresponds to form I crystal of chitosan. While, peak at 2θ = 15.12° and 21.9° represents form II crystals of chitosan (Chen, Yang, Gu, & Shao, 2001). S_3 showed a broad peak at 9.2° and 14.43° (2θ) which corresponds to the presence of amorphous form of chitosan in the membrane. Whereas, two sharp peaks at 19.12° and 23.24° (2θ) prove the presence of PEO crystals in the membrane (Zivanovic, Li, Davidson, & Kit, 2007). These diffraction peaks were observed with either shifted towards lower angle or with small broadening and decreased intensity. These circumstances further indicating the formation of hydrogen bonding between chitosan and PEO (Poonam, Dinesh Kumar, & Nirali, 2012).

3.2. Application of CPNM as adsorbent

3.2.1. Determination of best composition as adsorbent

For all three metal ions (Cu(II), Zn(II) and Pb(II)), maximum adsorption was noticed about 96%, 91% and 83% respectively after 60 min. Since Cu(II) adsorption reached equilibrium after 60 min, for further studies, 60 min was selected as control parameter.

Adsorption experimental results were tabulated in Table 2. From Table 2, for all three metal ions, removal (%) noticed as the following order $S_3 \square S_2 \square S_1 \square S_4 \square S_5$. As the adsorption capability depends on the specific surface area and hydrophilic nature, to prove this trend CPNM samples were further characterized by water contact angle measurement and surface area analysis.

Water contact angles and N_2 adsorption-desorption isotherm analysis of the CPNM samples were shown in Fig. 4.

From Fig. 4, the water contact angles of S_1, S_2, S_3, S_4 and S_5 were 48°, 35°, 27°, 65° and 85° respectively. It was reported that the beaded fibres tend to have a greater water contact angle due to the increased surface roughness resulted from the presence of beads (Ma, Mao, Gupta, Gleason, & Rutledge, 2005; Shao, Wu, & Xu, 2009). In this study the result showed that, beadless S_3 had the lowest contact angle. Therefore it is most hydrophilic among the CPNM samples. It is well known that, hydrophilicity increases the adsorption capacity of membrane (Rodrigues, LeVan, & Tondeur, 2012). Therefore S_3 had the maximum adsorption capability (Table 3).

From Fig. 4 it is noticeable that all five CPNM samples showed typical type IV N_2 adsoprtion-desorption isotherm which indicted the characteristic of mesoporous structure.

The specific surface area of S_1, S_2, S_3, S_4 and S_5 were found to be 187, 195, 218, 171 and 148 m^2/g respectively. Since S_3 had the largest specific surface area, this leads to the smallest water contact angle of S_3 (Huang et al., 2010). Moreover, larger surface area facilitates the adsorption process (Mangun, Daley, Braatz, & Economy, 1998; Zhang, Li, Liu, Sun, & Li, 2013), therefore S_3 had the maximum adsorption capability as it possessed largest specific surface area.

As a result, considering the hydrophilicity and specific surface area of CPNM samples, it can be concluded that, chitosan/PEO composition that lead to fabricate fibres with least number of beads tend to possess highest hydrophilicity and maximum specific surface area and, thus lead to the maximum adsorption capability. In this study S_3 (60:40 chitosan:PEO ratio) possessed the maximum adsorption capability.

The ability of S_3 as an adsorbent was further illustrated by applying adsorption kinetics and isotherm model. The equilibrium adsorption data was analysed on the removal of Cu(II), Zn(II) and Pb(II) ion.

3.2.2. Adsorption kinetics

The calculated kinetics parameters are tabulated in Table 3.

Comparing the χ^2 and R^2 values with pseudo second order plots indicated that adsorption of metal ions onto S_3 did not correspond to Lagergren first order kinetic model. On the other hand, by observing high R^2 (≤0.99) value and lower χ^2 value, it is obvious that, adsorption of metal ions onto S_3 follow pseudo second order kinetic model. This result is in agreement with other researchers' findings who indicated pseudo second order kinetic model is better fit for the adsorption process (Aydın & Aksoy, 2009; Dragan, Dinu, & Timpu, 2010). From Table 3, it is also very clear that, equilibrium capacity ($q_{e.cal}$) increases and rate constant (k_2) decreases with increasing metal ion concentrations. This inclination reveals that, for lower concentration, adsorption process takes shorter time to reach equilibrium. This trend is also compatible with other studies (Chang, Tsai, Ing, & Chang, 2003; Chen, Zhang, & Chen, 2010). The compatibility of Pseudo second order kinetic model of the metal ion adsorption onto nanofibrous membrane suggests that, both adsorbent and adsorbate are responsible for rate limiting step (Gedam & Dongre, 2015).

3.2.3. Intra particle diffusion

The plots of q_t versus $t^{1/2}$ for intraparticle diffusion model is shown in Fig. 5 (only the plots for 50 mg/L initial concentration is shown). According to Grabowska and Gryglewicz (Lorenc-Grabowska & Gryglewicz, 2007; Namasivayam & Kavitha, 2002), the plots may give a multi-linear curve.

From Fig. 5, for all three metal ions there are three linear portions present in the curve, meaning that more than one process is responsible for adsorption. First sharper portion denotes the diffusion of metal ion, which is boundary layer diffusion. The following two portions signify the intraparticle diffusion (Lorenc-Grabowska & Gryglewicz, 2007). Where the second portion denotes gradual adsorption of metal ions onto S_3 and the third one refers to the

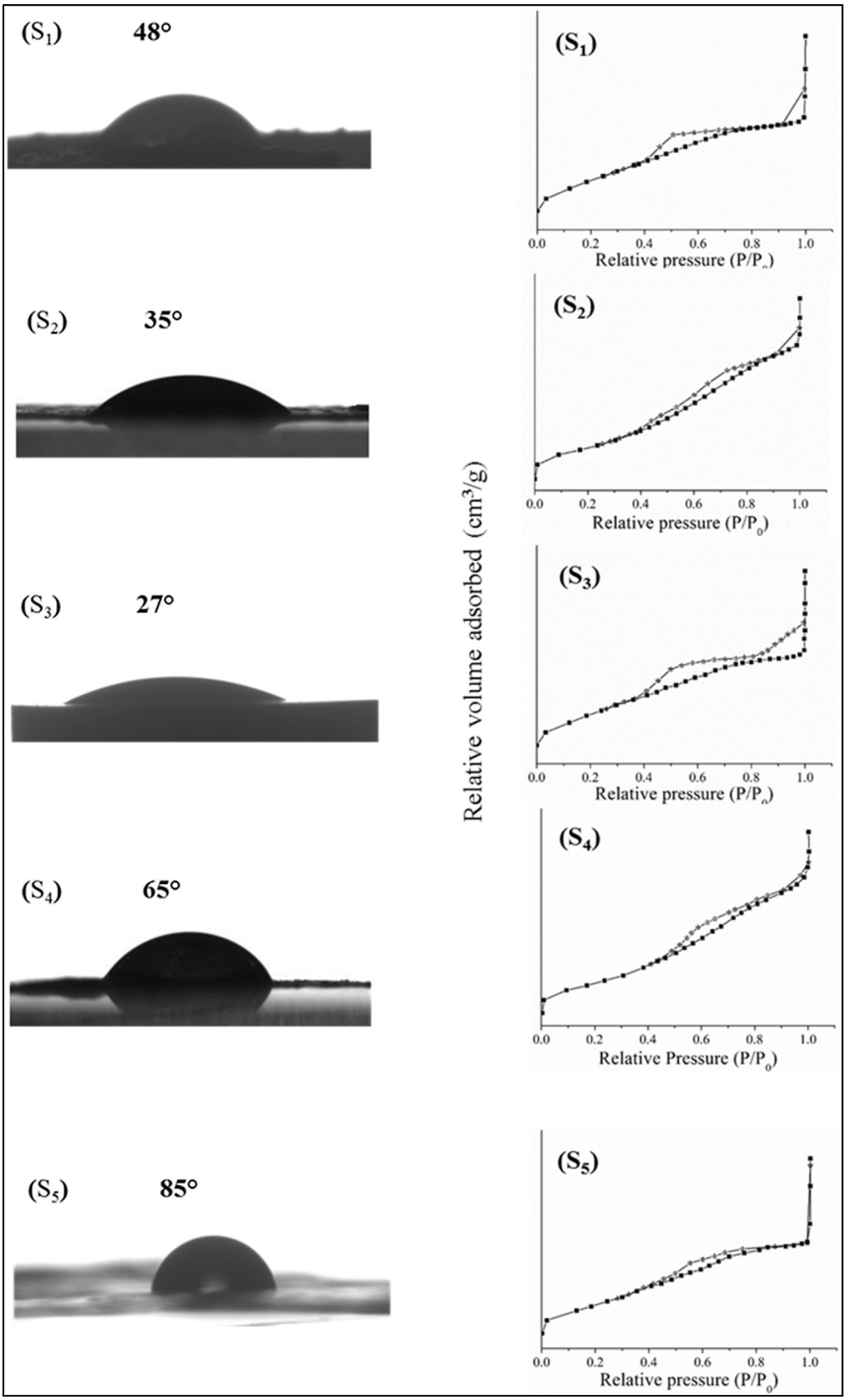

Fig. 4. Water contact angle and N_2 adsorption-desorption isotherm of CPNM.

equilibrium stage. At the equilibrium, due to the presence of very low metal ion concentration, intraparticle diffusion tends to slow down. The equilibrium plots do not pass through the origin, which signifies intraparticle diffusion is not only the rate limiting step, some boundary layer effect is also responsible (Gedam & Dongre, 2015). Diffusion co-efficient (k_s) value for Cu(II), Zn(II) and Pb(II)

Table 3
Kinetic parameters for the adsorption of heavy metal ions.

Metal ion	Conc. (mg/L)	q_e	Lagergren first order				Pseudo second order			
			$q_{e.cal}$	k_1	R^2	χ^2	$q_{e.cal}$	k_2	R^2	χ^2
Cu(II)	50	16.7	8.67	0.068	0.98	7.44	17.8	0.013	1	0.067
	100	32.03	24.15	0.181	0.98	2.57	35.21	0.005	0.99	0.287
	200	62.35	50.94	0.082	0.98	2.55	70.08	0.002	0.99	0.853
	300	88.65	108.31	0.099	0.98	3.56	101.17	0.001	1	1.57
Zn(II)	50	16.19	9.49	0.071	0.98	4.73	17.43	0.012	1	0.088
	100	30.33	19.66	0.077	0.98	5.79	33.10	0.006	0.99	0.231
	200	58.26	47.12	0.083	0.98	2.63	65.91	0.002	0.99	0.887
	300	81.5	93.84	0.093	0.98	1.62	84.43	0.001	0.99	0.102
Pb(II)	50	16.03	10.96	0.0734	0.96	2.34	17.42	0.011	0.99	0.11
	100	29.96	19.31	0.076	0.97	5.87	32.63	0.0009	0.99	0.159
	200	57.56	46.51	0.084	0.98	2.72	65.06	0.0002	0.99	0.86
	300	80.74	89.54	0.092	0.98	0.86	83.89	0.0001	0.99	0.118

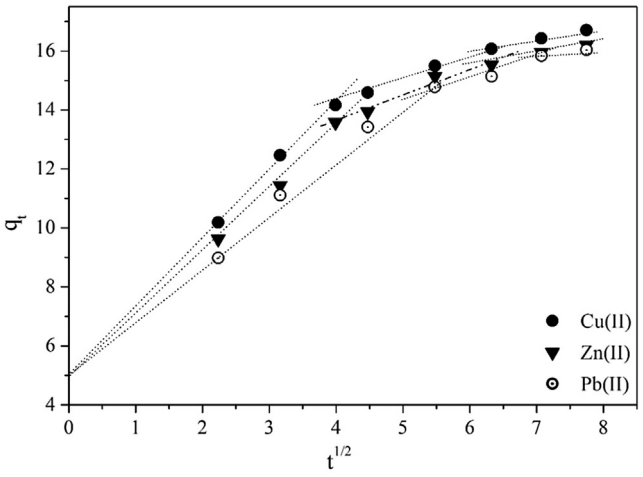

Fig. 5. Plots of q_t versus $t^{1/2}$ for Intraparticle diffusion model.

were found to be 0.10957, 0.09221 and 0.07245. Therefore, Cu(II) has the higher diffusion co-efficient (k_s), which leads it to reach equilibrium at shorter time compared to Zn(II) and Pb(II) ion.

3.2.4. Adsorption isotherm

The capacity of the adsorbent, surface properties and affinity of the adsorbents can be determined from equilibrium adsorption isotherms. Better agreement of equilibrium data with Freundlich isotherm signifies the heterogeneous systems and reversible adsorption process. Freundlich constant "n" denotes the type of adsorption. The value of "n" can be as follows: n = 1, n < 1 and n □ 1. These three values denotes the linear adsorption process, chemical adsorption process and physical adsorption process, respectively (Özcan, Erdem, & Özcan, 2005). Whereas, better agreement of equilibrium data with Langmuir isotherm signifies that the structure of adsorbent is homogeneous. According to Hall et al. (Hall, Eagleton, Acrivos, & Vermeulen, 1966), the equilibrium parameter R_L can have four different values, like: $R_L = 1$, $R_L = 0$, R_L □ 1 and $0 < R_L < 1$. These four values symbolizes linear adsorption, irreversible adsorption, unfavourable and favourable adsorption process, respectively. By comparing the linear regression correlation coefficient (R^2) value ($R^2 \leq 0.98$ for Freundlich isotherm and $R^2 \geq 0.98$ for Langmuir isotherm model), it is obvious that, the adsorption of heavy metal ions onto CPNM can be better described by Langmuir isotherm model. Therefore, it can be concluded that S_3 is homogeneous and mono layer adsorption condition exists during the adsorption process. The value of "n" is also found above unity, which signifies, adsorption of heavy metal ions onto S_3 is a physical adsorption process. The value of R_L is in between 0 and 1, proving the favourability of heavy metal ions at the experimental conditions. Approximately 120, 117 and 108 mg g^{-1} were the maximum adsorption capacity of S_3 for Cu(II), Zn(II) and Pb(II) ion respectively.

3.2.5. Reusability of the adsorbent

To evaluate the reusability of S_3 as an adsorbent, the adsorption test was repeated for five times for the same sample. Removal efficiency of S_3 for Cu(II), Zn(II) and Pb(II) ions were unchanged for the first three cycles, however, the efficiency reduced 0.75% and 1.31% in the fourth and fifth cycle, which was not significant. Slight reduction in efficiency may be due to the loss of some active groups during the acid wash of the sample. Therefore, it can be concluded that, S_3 can be reused without no significant loss in adsorption efficiency.

4. Conclusion

In this study, chitosan/PEO nanofibrous membrane having no beads, mesopores, and high specific surface area was successfully synthesized by electrospinning process. The formation of hydrogen bonding between the molecules of chitosan and PEO were substantiated by FTIR, and XRD analysis. Beadless fibres tend to show lowest contact angle and highest specific surface area, which are advantageous for the adsorption process. Based on the kinetic study, pseudo second order kinetic model was best suited with the experimental data. Whereas the comparative equilibrium isotherm experiments shows that, Langmuir isotherm can better describe the adsorption of metal ion. The maximum adsorption capacity for Cu(II), Zn(II) and Pb(II) ions were found to be 120, 117 and 108 mg g^{-1} respectively. The physical adsorption nature was proved by Freundlich isotherm constant value. Moreover, the beadless nanofibres can be reused without having no significant loss of adsorption capability.

Acknowledgements

The authors greatly appreciate the financial support from University of Malaya under the University of Malaya Research Grant (UMRG) fund (grant no. RP022C-13AET), Fundamental Research Graduate Scheme (FRGS) (grant no. FP026-2014B), Postgraduate Research Fund (PPP) (grant no. PG150-2015A) and Ministry of Higher Education through High Impact Research Grant (grant no. UM.C/625/1/HIR/MOHE/ENG/40).

References

Aydın, Y. A., & Aksoy, N. D. (2009). Adsorption of chromium on chitosan: Optimization, kinetics and thermodynamics. *Chemical Engineering Journal, 151*(1), 188–194.

Bhattarai, N., Edmondson, D., Veiseh, O., Matsen, F. A., & Zhang, M. (2005). Electrospun chitosan-based nanofibers and their cellular compatibility. *Biomaterials*, *26*(31), 6176–6184.

Cai, Z.-, Mo, X.-, Zhang, K.-, Fan, L.-, Yin, A.-, He, C.-, et al. (2010). Fabrication of chitosan/silk fibroin composite nanofibers for wound-dressing applications. *International Journal of Molecular Sciences*, *11*(9), 3529–3539.

Chakraborty, S., Chowdhury, S., & Saha, P. D. (2011). Adsorption of crystal violet from aqueous solution onto NaOH-modified rice husk. *Carbohydrate Polymers*, *86*(4), 1533–1541.

Chang, C., Tsai, W., Ing, C., & Chang, C. (2003). Adsorption of polyethylene glycol (PEG) from aqueous solution onto hydrophobic zeolite. *Journal of Colloid and Interface Science*, *260*(2), 273–279.

Chen, X., Yang, H., Gu, Z., & Shao, Z. (2001). Preparation and characterization of HY zeolite-filled chitosan membranes for pervaporation separation. *Journal of Applied Polymer Science*, *79*(6), 1144–1149.

Chen, Z., Mo, X., He, C., & Wang, H. (2008). Intermolecular interactions in electrospun collagen–chitosan complex nanofibers. *Carbohydrate Polymers*, *72*(3), 410–418.

Chen, D., Zhang, J., & Chen, J. (2010). Adsorption of methyl tert-butyl ether using granular activated carbon: Equilibrium and kinetic analysis. *International Journal of Environmental Science & Technology*, *7*(2), 235–242.

Cui, L., Xiong, Z., Guo, Y., Liu, Y., Zhao, J., Zhang, C., et al. (2015). Fabrication of interpenetrating polymer network chitosan/gelatin porous materials and study on dye adsorption properties. *Carbohydrate Polymers*, *132*, 330–337.

Deitzel, J., Kleinmeyer, J., Harris, D., & Tan, N. B. (2001). The effect of processing variables on the morphology of electrospun nanofibers and textiles. *Polymer*, *42*(1), 261–272.

Desai, K., & Kit, K. (2008). Effect of spinning temperature and blend ratios on electrospun chitosan/poly (acrylamide) blends fibers. *Polymer*, *49*(19), 4046–4050.

Domszy, J. G., & Roberts, G. A. (1985). Evaluation of infrared spectroscopic techniques for analysing chitosan. *Die Makromolekulare Chemie*, *186*(8), 1671–1677.

Dong, Y., Xu, C., Wang, J., Wu, Y., Wang, M., & Ruan, Y. (2002). Influence of degree of deacetylation on critical concentration of chitosan/dichloroacetic acid liquid-crystalline solution. *Journal of Applied Polymer Science*, *83*(6), 1204–1208.

Dotto, G., & Pinto, L. (2011). Adsorption of food dyes onto chitosan: Optimization process and kinetic. *Carbohydrate Polymers*, *84*(1), 231–238.

Dragan, E. S., Dinu, M. V., & Timpu, D. (2010). Preparation and characterization of novel composites based on chitosan and clinoptilolite with enhanced adsorption properties for Cu 2+. *Bioresource Technology*, *101*(2), 812–817.

Duan, B., Yuan, X., Zhu, Y., Zhang, Y., Li, X., Zhang, Y., et al. (2006). A nanofibrous composite membrane of PLGA–chitosan/PVA prepared by electrospinning. *European Polymer Journal*, *42*(9), 2013–2022.

Gaharwar, A. K., Mihaila, S. M., Kulkarni, A. A., Patel, A., Di Luca, A., Reis, R. L., et al. (2014). Amphiphilic beads as depots for sustained drug release integrated into fibrillar scaffolds. *Journal of Controlled Release*, *187*, 66–73.

Gedam, A. H., & Dongre, R. S. (2015). Adsorption characterization of Pb (ii) ions onto iodate doped chitosan composite: Equilibrium and kinetic studies. *RSC Advances*, *5*(67), 54188–54201.

Haider, S., & Park, S.-Y. (2009). Preparation of the electrospun chitosan nanofibers and their applications to the adsorption of Cu (II) and Pb (II) ions from an aqueous solution. *Journal of Membrane Science*, *328*(1), 90–96.

Hall, K. R., Eagleton, L. C., Acrivos, A., & Vermeulen, T. (1966). Pore-and solid-diffusion kinetics in fixed-bed adsorption under constant-pattern conditions. *Industrial & Engineering Chemistry Fundamentals*, *5*(2), 212–223.

Han, R., Zhang, L., Song, C., Zhang, M., Zhu, H., & Zhang, L. (2010). Characterization of modified wheat straw, kinetic and equilibrium study about copper ion and methylene blue adsorption in batch mode. *Carbohydrate Polymers*, *79*(4), 1140–1149.

Hardiansyah, A., Tanadi, H., Yang, M.-C., & Liu, T.-Y. (2015). Electrospinning and antibacterial activity of chitosan-blended poly (lactic acid) nanofibers. *Journal of Polymer Research*, *22*(4), 1–10.

Hassiba, A. J., El Zowalaty, M. E., Nasrallah, G. K., Webster, T. J., Luyt, A. S., Abdullah, A. M., et al. (2016). Review of recent research on biomedical applications of electrospun polymer nanofibers for improved wound healing. *Nanomedicine*, *11*(6), 715–737.

Ho, Y.-S. (2004). Selection of optimum sorption isotherm. *Carbon*, *42*(10), 2115–2116.

Homayoni, H., Ravandi, S. A. H., & Valizadeh, M. (2009). Electrospinning of chitosan nanofibers: Processing optimization. *Carbohydrate Polymers*, *77*(3), 656–661.

Huang, Z.-M., Zhang, Y.-Z., Kotaki, M., & Ramakrishna, S. (2003). A review on polymer nanofibers by electrospinning and their applications in nanocomposites. *Composites Science and Technology*, *63*(15), 2223–2253.

Huang, F., Wang, Q., Wei, Q., Gao, W., Shou, H., & Jiang, S. (2010). Dynamic wettability and contact angles of poly (vinylidene fluoride) nanofiber membranes grafted with acrylic acid. *Express Polymer Letters*, *4*, 551–558.

Irani, M., Amjadi, M., & Mousavian, M. A. (2011). Comparative study of lead sorption onto natural perlite, dolomite and diatomite. *Chemical Engineering Journal*, *178*, 317–323.

Järup, L. (2003). Hazards of heavy metal contamination. *British Medical Bulletin*, *68*(1), 167–182.

Kohsari, I., Shariatinia, Z., & Pourmortazavi, S. M. (2016). Antibacterial electrospun chitosan–polyethylene oxide nanocomposite mats containing bioactive silver nanoparticles. *Carbohydrate Polymers*, *140*, 287–298.

Koosha, M., Mirzadeh, H., Shokrgozar, M. A., & Farokhi, M. (2015). Nanoclay-reinforced electrospun chitosan/PVA nanocomposite nanofibers for biomedical applications. *RSC Advances*, *5*(14), 10479–10487.

Li, K., Sun, H., Sui, H., Zhang, Y., Liang, H., Wu, X., et al. (2015). Composite mesoporous silica nanoparticle/chitosan nanofibers for bone tissue engineering. *RSC Advances*, *5*(23), 17541–17549.

Lin, Y.-F., & Chang, C.-Y. (2014). Magnetic mesoporous iron oxide/carbon aerogel photocatalysts with adsorption ability for organic dye removal. *RSC Advances*, *4*(54), 28628–28631.

Liu, H., & Wang, C. (2014). Chitosan scaffolds for recyclable adsorption of Cu (ii) ions. *RSC Advances*, *4*(8), 3864–3872.

Lorenc-Grabowska, E., & Gryglewicz, G. (2007). Adsorption characteristics of Congo Red on coal-based mesoporous activated carbon. *Dyes and Pigments*, *74*(1), 34–40.

Ma, M., Mao, Y., Gupta, M., Gleason, K. K., & Rutledge, G. C. (2005). Superhydrophobic fabrics produced by electrospinning and chemical vapor deposition. *Macromolecules*, *38*(23), 9742–9748.

Mangun, C., Daley, M., Braatz, R., & Economy, J. (1998). Effect of pore size on adsorption of hydrocarbons in phenolic-based activated carbon fibers. *Carbon*, *36*(1), 123–129.

Mi, F.-L., Wu, S.-J., & Chen, Y.-C. (2015). Combination of carboxymethyl chitosan-coated magnetic nanoparticles and chitosan-citrate complex gel beads as a novel magnetic adsorbent. *Carbohydrate Polymers*, *131*, 255–263.

Min, B.-M., Lee, S. W., Lim, J. N., You, Y., Lee, T. S., Kang, P. H., et al. (2004). Chitin and chitosan nanofibers: Electrospinning of chitin and deacetylation of chitin nanofibers. *Polymer*, *45*(21), 7137–7142.

Miya, M., Iwamoto, R., Yoshikawa, S., & Mima, S. (1980). Ir spectroscopic determination of CONH content in highly deacylated chitosan. *International Journal of Biological Macromolecules*, *2*(5), 323–324.

Muzzarelli, R. A., Tanfani, F., Scarpini, G., & Laterza, G. (1980). The degree of acetylation of chitins by gas chromatography and infrared spectroscopy. *Journal of Biochemical and Biophysical Methods*, *2*(5), 299–306.

Namasivayam, C., & Kavitha, D. (2002). Removal of Congo Red from water by adsorption onto activated carbon prepared from coir pith, an agricultural solid waste. *Dyes and Pigments*, *54*(1), 47–58.

Özcan, A. S., Erdem, B., & Özcan, A. (2005). Adsorption of acid blue 193 from aqueous solutions onto BTMA-bentonite. *Colloids and Surfaces A: Physicochemical and Engineering Aspects*, *266*(1), 73–81.

Ozdemir, O., Armagan, B., Turan, M., & Celik, M. S. (2004). Comparison of the adsorption characteristics of azo-reactive dyes on mezoporous minerals. *Dyes and Pigments*, *62*(1), 49–60.

Pittarate, C., Yoovidhya, T., Srichumpuang, W., Intasanta, N., & Wongsasulak, S. (2011). Effects of poly (ethylene oxide) and ZnO nanoparticles on the morphology, tensile and thermal properties of cellulose acetate nanocomposite fibrous film. *Polymer Journal*, *43*(12), 978–986.

Poonam, S., Dinesh Kumar, K., & Nirali, G. (2012). Effect of nano-filler on structural and ionic transport properties of plasticized polymer electrolyte. *Open Journal of Organic Polymer Materials*, *2012*.

Rakkapao, N., Vao-soongnern, V., Masubuchi, Y., & Watanabe, H. (2011). Miscibility of chitosan/poly (ethylene oxide) blends and effect of doping alkali and alkali earth metal ions on chitosan/PEO interaction. *Polymer*, *52*(12), 2618–2627.

Rodrigues, A. E., LeVan, M. D., & Tondeur, D. (2012). *Adsorption: Science and technology*. Springer Science & Business Media.

Sannan, T., Kurita, K., Ogura, K., & Iwakura, Y. (1978). Studies on chitin: 7. IR spectroscopic determination of degree of deacetylation. *Polymer*, *19*(4), 458–459.

Shao, L.-, Wu, J., & Xu, Z.-. (2009). Electrospraying/electrospinning of poly (γ-STEARYL-L-GLUTAMATE): formation of surfaces with superhydrophobicity. *Chinese Journal of Polymer Science*, *27*(01), 115–120.

Shigemasa, Y., Matsuura, H., Sashiwa, H., & Saimoto, H. (1996). Evaluation of different absorbance ratios from infrared spectroscopy for analyzing the degree of deacetylation in chitin. *International Journal of Biological Macromolecules*, *18*(3), 237–242.

Sun, X.-F., Liu, B., Jing, Z., & Wang, H. (2015). Preparation and adsorption property of xylan/poly (acrylic acid) magnetic nanocomposite hydrogel adsorbent. *Carbohydrate Polymers*, *118*, 16–23.

Talebian, S., Afifi, A., & Khanlou, H. (2014). Fabrication and characterisation of chitosan/poly vinyl alcohol nanofibres via electrospinning. *Materials Research Innovations*, *18*(S6) [S6- 331-S336-335].

Thavasi, V., Singh, G., & Ramakrishna, S. (2008). Electrospun nanofibers in energy and environmental applications. *Energy & Environmental Science*, *1*(2), 205–221.

Xiao, S., Ma, H., Shen, M., Wang, S., Huang, Q., & Shi, X. (2011). Excellent copper (II) removal using zero-valent iron nanoparticle-immobilized hybrid electrospun polymer nanofibrous mats. *Colloids and Surfaces A: Physicochemical and Engineering Aspects*, *381*(1), 48–54.

Zhang, M., Li, L., Liu, J., Sun, Y., & Li, G. (2013). Surface characteristics of alkali modified activated carbon and the adsorption capacity of methane. *Huan jing ke xue = Huanjing kexue/[bian ji, Zhongguo ke xue yuan huan jing ke xue wei yuan hui Huan jing ke xue bian ji wei yuan hui.]*, *34*(1), 39–44.

Zivanovic, S., Li, J., Davidson, P. M., & Kit, K. (2007). Physical, mechanical, and antibacterial properties of chitosan/PEO blend films. *Biomacromolecules*, *8*(5), 1505–1510.